Intercalation-Induced Topotactic Phase Transformation of Tungsten Disulfide Crystals

A K M Manjur Hossain[1], Joseph McBride[1], Masoumeh Mahmoudi Gahrouei[1], Sabin Gautam[2], Jefferson A Carter[2], Piumi Indrachapa Samarawickrama[2], John F Ackerman[3,5], Laura Rita de Sousa Oliveira[1], Jinke Tang[2,4], Jifa Tian[2,4] and Brian M Leonard[1]

1. Department of Chemistry, University of Wyoming, Laramie, Wyoming, USA
2. Department of Physics and Astronomy, University of Wyoming, Laramie, Wyoming, USA
3. Department of Chemical and Biological Engineering, University of Wyoming, Laramie, Wyoming, USA
4. Center for Quantum Information Science & Engineering, University of Wyoming, Laramie, Wyoming, USA
5. Resonant Sciences Beaver Creek, Ohio, USA

ABSTRACT: Recent research has demonstrated the potential for topological superconductivity, anisotropic Majorana bound states, optical nonlinearity, and enhanced electrochemical activity for 2M phases of transition metal dichalcogenides (TMDs). However, these unique TMD compounds exhibit metastability and upon heating undergo a transition to the thermodynamically stable 2H phase. Thus, the growth of large 2M WS_2 crystals has remained quite challenging. To overcome this issue, a novel synthetic method was developed, focusing on a molten salt reaction

to synthesize large 2H crystals and then inducing transformation to the 2M phase through intercalation and thermal treatment. The 2H crystals were intercalated via a room-temperature sodium naphthalenide solution, producing a previously unreported Na intercalated 2H WS_2 phase. Thermal heating was required to facilitate the phase transition to the intercalated 2M crystal structure. This phase transition was followed by X-ray Diffraction (XRD), Scanning electron microscopy (SEM), electron dispersive X-ray spectroscopy (EDS), and Raman spectroscopy which confirmed the synthesis of the intercalated 2M phase. Upon deintercalation, crystal and powder samples showed superconductivity with a Tc of 8.6-8.7 K, similar to previously reported values. The generality of this process was further demonstrated using alkali metal triethyl borohydride to intercalate 2H WS_2 and produced the desired 2M phase.

Introduction

Research into layered two-dimensional (2D) materials has enabled several exciting technological applications, including optoelectronics, wearable electronics, energy storage, catalysis, and superconductivity[1–9]. Transition metal dichalcogenides (TMDs), which are composed of a transition metal and chalcogenide atoms (typically S, Se, or Te), are among the most heavily investigated 2D materials for these applications. TMDs usually adopt a few different crystal structures, including hexagonal (2H), trigonal (1T), orthorhombic (T_d), and monoclinic (2M or 1T′) with different stacking arrangments[10]. The differences in these structures can be viewed either as local coordination of the chalcogenide around the metal center (octahedral or trigonal prismatic) or long-range, i.e., ordering of the layers separated by a van der Waals (vdW) gap. The presence of heavy transition metal atoms can introduce strong spin-orbit coupling in these TMDs, resulting in novel topological properties. Among those structures,

semiconducting 2H TMDs have been studied for their valley polarization found in MoS_2 and monolayers of $NbSe_2$, which have shown ising superconductivity[11,12]. The quantum spin hall effect was also found in the monolayers of 2M WS_2, 1T′ WTe_2, and 1T′ WSe_2[13–15].

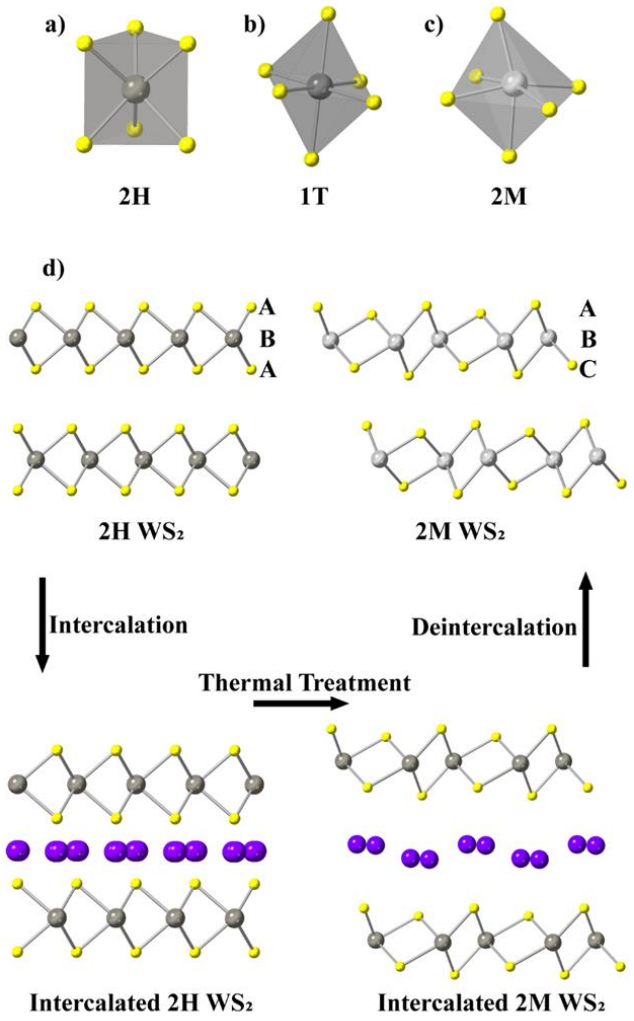

Figure 1: a), b), and c) WS_6 polyhedra for 2H, 1T, and 2M phases of WS_2. d) Schematic demonstrating the conversion of 2H to intercalated 2H, intercalated 2M and finally 2M WS_2.

WS_2 has recently garnered significant interest due to its ability to undergo engineered-phase conversion, leading to unique phase-dependent properties [16–19]. 2H WS_2 features tungsten

surrounded by 6 sulfurs in a trigonal prism (Figure 1a) giving rise to a honeycomb crystal structure analogous to graphene with S-W-S atomic layers, forming an A-B-A stacking sequence (Figure 1d)[20].1T phase has tungsten surrounded by 6 sulfurs (Figure 1b) in an octahedra geometry and exhibits a different stacking arrangement with A-B-C repeating layers (Figure 1d). With further distortion of the tungsten octahedra, the 1T WS_2 structure can be visually transformed to the related 2M or 1T′ structures. 2M WS_2 is a unique structure formed with distinctive in-plane W-W zigzag chains. Recently, 2M WS_2 was shown to have a superconductivity transition temperature of 8.8K, which is the highest superconducting temperature observed among TMDs[2]. However, synthesizing the 2M phase of WS_2 remains challenging due to its tendency to revert to the more stable 2H phase[6].

Intercalation chemistry has previously been used to modify TMDs, including exfoliation of monolayers and alteration of the crystal structure of the host materials[21–23]. n-butyllithium is frequently used to intercalate Li into the vdW region, followed by hydration to aid in the exfoliation of a few layer samples[4,24]. Similarly, Li, Na, and K metals were intercalated through their naphthalene adducts and used to exfoliate TMDs[21,22]. While the crystal structure of potassium intercalated WS_2 ($K_{0.36}WS_2$) has been reported to have a layered structure reminiscent of the 2M structure, there is very limited data or understanding of this intercalated phase[25]. Similarly, an intercalated $Rb_{0.21}WS_2$ crystal structure with a 2M layered structure has been reported without further investigation into its properties[26].

In previous reports about 2M WS_2, samples were synthesized through high-temperature intercalation of potassium into 2H WS_2, indicating that this reported K_xWS_2 compound served as an intermediate phase and is critical to the formation of the 2M phase. The desired 2M crystal structure can be isolated upon deintercalation of the potassium. While this intercalation-

deintercalation process can reproducibly result in powders of 2M WS_2, the synthesis of larger crystals has remained quite challenging. The long growth time and slow cooling process required for crystal growth have also proven difficult due to potassium etching the quartz tubes, resulting in oxygen-exposed samples and failed reactions.

To overcome these limitations, we have developed a novel method for structural conversion of 2H WS_2 to 2M through low-temperature, solution-based intercalation reactions. Through this process, two unique intercalated phases of WS_2 were identified, indicating that this process is more complex than the simple intercalation of potassium. To better understand this mechanism, naphthalene adducts of alkali metals (MNapth) were used as reducing agents and subsequent intercalation reagents. The intercalation process begins via the reduction of tungsten, which facilitates the intercalation of the alkali metal into the vdW region to charge balance the reduced tungsten[27]. Upon intercalation, the 2H WS_2 phase forms a previously unreported alkali metal intercalated 2H phase. To complete the phase transformation, thermal treatment of the intercalated 2H phase is required to form the 2M MWS_2 (M=Na, K) and finally 2M WS_2 after deintercalation. Previous reports of 2M WS_2 and 2M WSe_2 utilized high-temperature intercalation reactions around 800-850°C, which is consistent with the required thermal treatments observed in this investigation[2,6,28,29]. However, the major advantage of this method is the reduction in annealing time due to the conversion of crystals rather than the growth of new crystals. Since alkali metals attack the quartz reaction vessels, shorter reaction times at high temperatures have a much higher rate of success in producing high quality centimeter sized crystals.

To demonstrate the generality of the naphthalenide method, the conversion reaction on both powders and crystals, using Na and K as the intercalated cations with all samples forming the

desired 2M WS_2. Additionally, a second set of reducing agents, metal triethyl borohydride (MTEBH) was used to perform the intercalation reactions and subsequently produced the same 2M phase as a final product.

Experimental Section

2H WS_2 Powder and Crystal synthesis

The 2H WS_2 powder was synthesized from elemental reagents with a stoichiometric 1:2 ratio for tungsten and sulfur. The reagents were placed in a quartz tube, vacuum sealed, and heated to 1100˚C for nine days in a box furnace. Large cm-sized 2H crystals were synthesized through a previously reported molten salt flux method[30]. A 10g mixture of NaCl and CsCl with 38 mol % and 62 mol % was combined with WS_2 in an 18 cm long and 10mm diameter quartz tube. The polycrystalline WS_2 was pressed into the pellet prior to being placed in the tube with the salt flux. The tube was vacuum sealed and placed in a tube furnace where it was heated to 1100˚C at a 90˚C/hour rate and kept at that temperature for seven days. The tube was then cooled to 650˚C at a 2˚C/hour rate and quenched in a vertical orientation to separate salt flux from the resulting crystals produced at the cooler end of the tube. The crystals were washed with distilled water and ethanol several times to remove the salt flux, followed by drying at 90 ˚C for 24 hours.

Intercalation-induced phase transformation of 2H-WS_2 powder and crystals

Alkali metal naphthalenide (MNapth) solutions was formed by mixing 0.23 g Na metal and 0.5 g naphthalene in THF (for K Napth, 0.38 g K and 0.6 g naphthalene were used). After 24 hours of mixing, 2H WS_2 powders or crystals were added to the reactions. The powders were stirred

throughout the intercalation process, but the crystals were reacted without stirring to maintain the dimensions of the large crystals.

Alternatively, metal triethyl borohydride (MTEBH) reagents, were mixed with 2H WS_2 powders or crystals in a stainless-steel bomb reactor and heating it to 200˚C for five days. The stoichiometric ratio was maintained at 1 to 2.5 for powder 2H-WS_2 to MTEBH.

After intercalation, the resulting products were washed with 40 ml of THF 2-3 times and dried. To transform the intercalated samples to the 2M structure, the metal intercalated powders were heated to 800˚C at a rate of 100˚C/hour for 48 hours, while crystals were flash heated to 800˚C for 3 hours.

Deintercalation process

Both powders and crystals were deintercalated using a previously reported process utilizing 0.01M $K_2Cr_2O_7$ in 0.02M H_2SO_4[2]. The ratio of metal intercalated samples to the deintercalation solution was maintained at approximately 0.1g to 80 ml at room temperature for 1 hour while stirring every 10 minutes. The resulting samples were washed 3 to 4 times with 50 mL of distilled water and dried under a vacuum.

An alternate route for the deintercalation process was also pursued to avoid Cr deposition on the samples. In 50ml of 1M H_2SO_4, 0.1g intercalated samples were charged, and occasional slow stirring was maintained over 4 hours at 100˚C. The deintercalated crystals from the first process had better quality; however, the second process was typically followed to avoid surface deposition of Cr in the previous methods, which was shown to be as high as 5% (SI Figure 1).

Characterization

XRD

All sample preparation was done in an argon-filled glovebox where the O_2 and H_2O levels were maintained at less than 0.1 ppm. Air-free XRD samples were prepared using a glass sample holder covered with mylar film and sealed with vacuum grease. XRD data was collected using a Rigaku Smart Lab X-ray diffractometer with Cu-kα X-rays (1.5406Å).

SEM and EDS

SEM and EDS were analyzed using ThermoFisher Helios 5 UX and FEI Quanta 250.

Raman

Raman analysis was conducted in a Horiba Raman microscope with a 532 nm laser. 0.06mW power was used to acquire all the Raman spectra to avoid heating or any laser irradiation-induced phase transition. The silicon Raman modes at 520.52 cm^{-1} were used to calibrate the Raman microscope before each measurement.

TEM

Transmission electron microscopy (TEM) images and Selective area electron diffraction (SAED) patterns of 2H and 2M WS_2 were taken using a ThermoFisher Talos 200x. The samples are prepared by grinding in mortar for a few minutes, followed by sonication using THF. Then, thin crystals were drop-casted on copper grids.

Magnetic measurements

Magnetization measurements were conducted on the resulting 2M WS_2 using a Quantum Design Dynacool Physical Properties Measurement System (PPMS) Vibrating Sample Magnetometer (VSM) at the Colorado State University Analytical Resources Core.

Theoretical Calculations method

Density functional theory (DFT) calculations are performed using the Vienna *ab initio* simulation package (VASP) with the generalized gradient approximation (GGA), the Perdew–Burke–Ernzerhof (PBE) functional, and a cutoff energy of 500 eV for the plane-wave basis set[31–33]. The energy and force tolerances on each atom are set to 10^{-8} eV and 10^{-4} eV/Å, respectively. The DFT-D3 method of Grimme et al. with a zero-damping function for the vdW (dispersion) correction is applied[34]. A Monkhorst–Pack sampling of 5×5×4 and 4×5×5 k-points is used for the 2H and 2M phases. The lattice constants and angles corresponding to the 2H and 2M phases of WS_2 and 2H $K_{0.5}WS_2$ and M $K_{0.25}WS_2$ unit cells, are shown in SI Table 1. The tetrahedron method is adopted for the density of states (DOS) calculation and implemented with 7×7×6 and 6×7×7 k-points for 2H and 2M phases respectively. Phonon dispersions are obtained by implementing the frozen phonon method with the PHONOPY code (with a displacement amplitude of 0.01 Å for each atomic displacement)[35]. Unless otherwise specified, supercells of 3×3×2 are used for both the 2H and 2M phase geometries, in that order. The cohesive energy (E_{COH}) is calculated by using the expression:

$$E_{COH} = \frac{E_{tot} - \sum_{i=1}^{\alpha} n_i E_i}{N}, \qquad (1)$$

where E_{tot} is the total energy of the unit cell, n_i and E_i are the total numbers of atoms of type i and the energy of a single atom of type i in the gas phase, respectively. The sum of $n_i E_i$ is performed for all the different atom types, α, which is 2 for WS_2 or 3 for K_xWS_2.

Results and Discussion

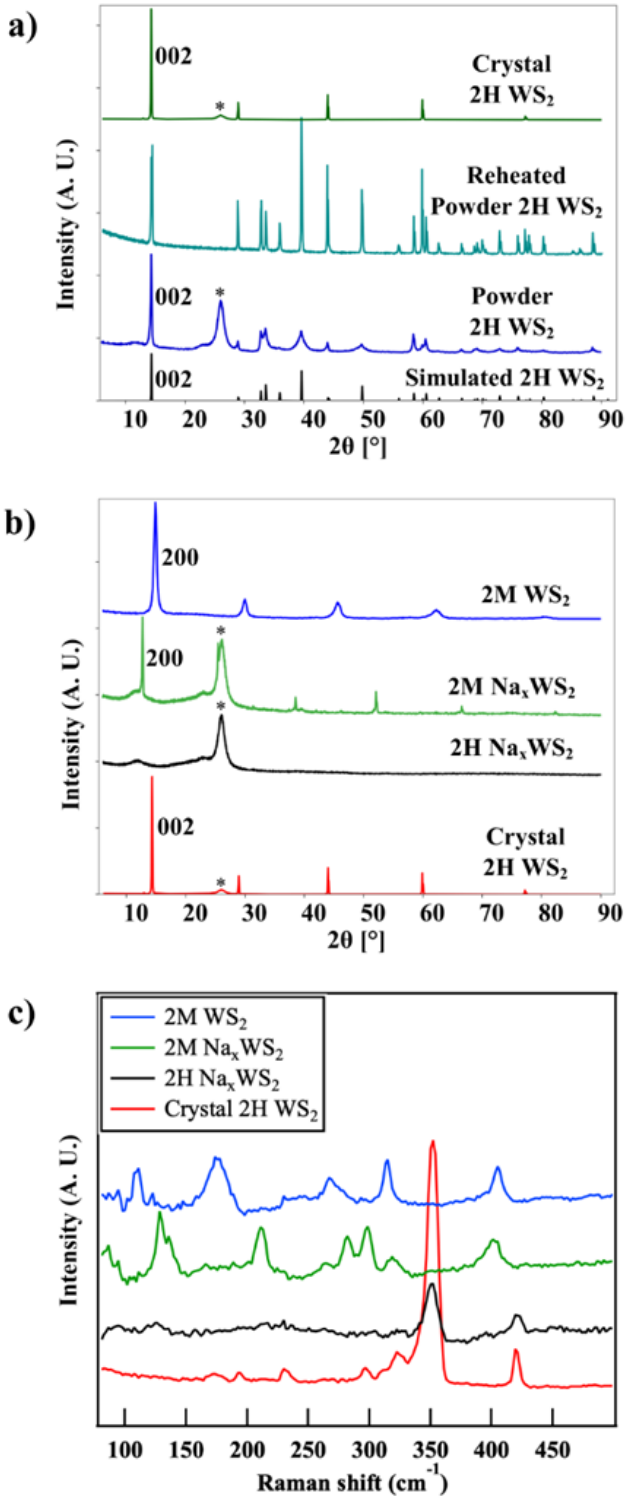

Figure 2: a) XRD data of synthesized 2H WS_2 powder and crystals with previously simulated data[36]. b) XRD of the four phases isolated in 2H to 2M WS_2 crystals conversion through the Na Naphthalenide route. c) Raman stacking of the four isolated phases during 2H to 2M WS_2 conversion through the Na Naphthalenide route. * Denotes the characteristic peak at 26° two theta from the mylar film, which was used to prepare the air and moisture free sample.

2H WS_2 powder was synthesized using stoichiometric mixtures of elemental W and S. Phase purity of the synthesized 2H WS_2 powders and crystals was determined through XRD, SEM, elemental analysis via EDS, Raman spectroscopy (Figure 2a, 3a, SI Figure 2). XRD of 2H WS_2 powders showed broad diffraction peaks that matched with calculated data for the 2H phase, as seen in Figure 2a. The WS_2 powder obtained from these reactions was further reacted at 1100°C to produce a highly crystalline powder, which was used for crystal growth due to better transport of WS_2 during the salt flux synthesis. The highly crystalline powders were combined with a NaCl-CsCl salt flux to synthesize centimeter-sized crystals and heated to 1100°C. Analysis of the XRD data for the large crystals shows primarily the layering 00l peaks, indicating preferential growth of crystals along the perpendicular to the stacking direction. The other hkl peaks are challenging to monitor due to the preferential orientation of the samples during the sample preparation of the WS_2 materials in the XRD sample holder. For simplicity, XRD analysis primarily focuses on the layering 00l peaks for pure 2H and intercalated 2H samples and h00 peaks for the intercalated 2M and pure 2M samples.

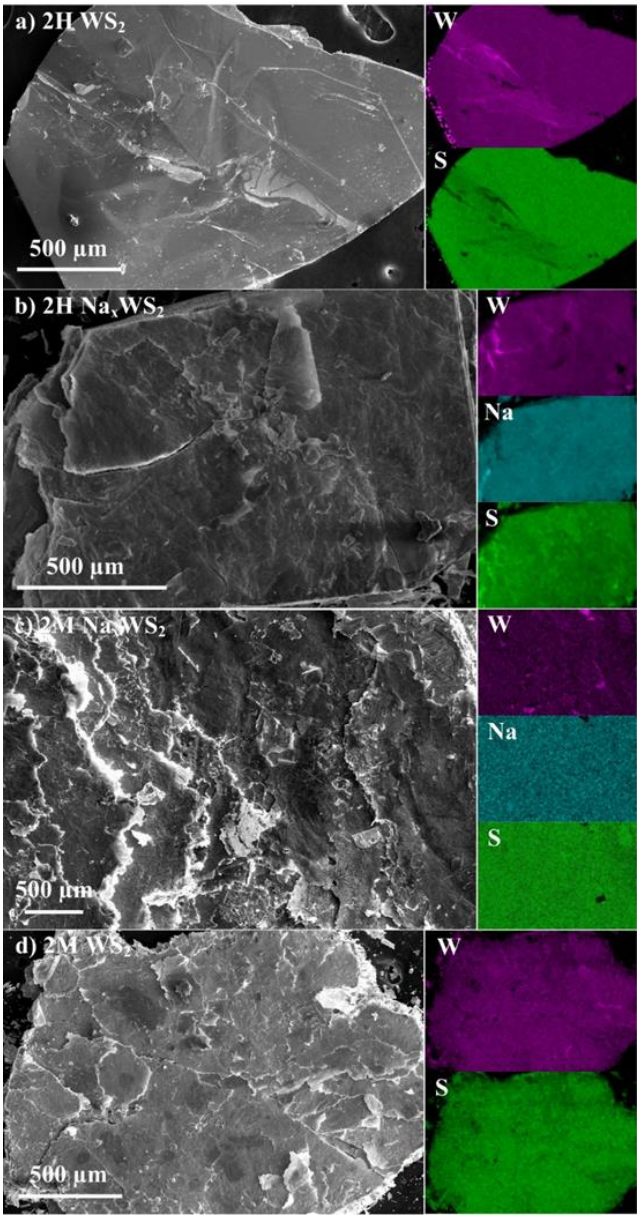

Figure 3: SEM images and EDS mapping of a) Pure 2H WS_2 crystals synthesized through salt flux reaction, b) Na intercalated 2H WS_2 crystals, c) Na intercalated 2M WS_2 crystals after flash heating, d) deintercalated 2M WS_2 crystals from Na Naphthalenide route.

SEM analysis of the synthesized 2H crystals showed layered hexagonal plate-like morphology, as seen in Figure 3. EDS of both crystals (Figure 3a) and powder (SI Figure 2) show a 1:2 ratio of W and S consistent with a stoichiometric ratio for WS_2. The hexagonal shape of the crystals and crystallites in the powder, combined with the 00l-dominated XRD, indicates these crystals are single phase with limited defects.

2M WS_2 conversion

The synthesized WS_2 powders and crystals were used to study the intercalation and phase conversion (Figure 2b, SI Figure 5). The crystals and powders were intercalated at room temperature using MNapth (Na, K). Upon addition of the 2H WS_2 to the reaction solution, the MNapth transfers an electron to the WS_2, reducing W and subsequently inserting metal ions into the vdW region of WS_2[22].

$C_{10}H_8 + xA \rightarrow x[A(C_{10}H_8)]$

$xA^+ + xe^- + WS_2 \rightarrow A_xWS_2$

M= Na, K

XRD of the Na intercalated 2H WS_2 in Figure 2b showed a disordered structure with a large lattice expansion due to the insertion of Na ions in the vdW region. While SEM and EDS showed Na fully intercalated the 2H phase, deintercalation of these low-temperature alkali metal intercalated WS_2 samples resulted in the 2H phase by XRD (SI Figure 4) indicating that the phase transition is more complicated than a simple reduction-intercalation process.

Based on this, the intercalated powders and crystals were then subjected to thermal treatment at 800ºC, which allowed complete conversion of the crystal's structure to the previously reported intercalated 2M phase. This conversion process is reasonably delicate with lower heating temperatures (700-750°C) resulting in the presence of 2 different intercalated phases (2H and 2M) and with higher temperatures (>850°C), annealing frequently showing thermal deintercalation and relaxation to the 2H phase. After thermal treatment, the crystal and powder samples were deintercalated, resulting in 2M WS_2, as shown in Figure 2b.

The XRD, EDS, and Raman spectroscopy monitored the phase transition from 2H to 2M. XRD data initially shows the metal intercalated WS_2 crystals retained a similar hexagonal structure to the starting 2H phase with an expansion of the c lattice parameter due to the insertion of Na into the vdW region. These crystal samples showed a high degree of disorder in both intercalated powder (SI Figure 5) and crystals WS_2 (Figure 2b), and little structural information could be confirmed from the XRD data other than this expansion. The sodium content was investigated via EDS, and the metal's distribution was also uniform (Figure 3b) with a Na to W ratio of 1 to 3 in the intercalated crystals both on the surface and after exfoliation via tape.

After thermal treatment, the crystals converted to an intercalated phase with an expanded lattice constant similar to the reported potassium intercalated WS_2 phase ($K_{0.36}WS_2$). While the crystal structure for the Na intercalated phase is not known, a similar Rb intercalated phase ($Rb_{0.21}WS_2$) has also been reported with a similar structure, allowing us to simulate a Na intercalated phase[26]. During the heating process, some alkali metals were deintercalated, as observed by a lower alkali metal content and evidence of etching the quartz tubing used for the reaction vessels. The W to Na ratio was 1 to 0.46 in this intercalated 2M phase with uniform Na distribution (Figure 3c). The lattice constant for the Na intercalated 2M WS_2 phase was

calculated to be 15.205Å, which decreased to 12.964Å after deintercalation (Figure 2b), resulting in the desired 2M phase. The deintercalated 2M WS_2 crystals showed a 1:2 ratio of W to S via EDS mapping and no Na present, indicating that the 2M phase was successfully deintercalated on these few mm-sized crystals (Figure 3d). The deintercalation process can be more difficult on larger crystals due to longer diffusion distances and lower surface area, and thus, the Na content should be monitored to ensure impurity-free 2M crystals. Some cracking was observed in the final 2M crystals, and a detailed investigation also showed some needle-shaped crystals, which is characteristic of the monoclinic phase of WS_2 (SI Figure 1). This is likely due to the stress induced upon phase conversion of the large crystals, and while this is a topotactic reaction, the crystals likely degrade slightly throughout the process. Single crystal diffraction was attempted on these samples; however, there was a large degree of disorder about the stacking axis resulting in poor data.

The intercalated powders showed more extensive expansion when exposed to air which is likely due to hydration of the alkali metal ions (SI Figure 6). This hydration is similar to the previously reported $K_{0.36}(H_2O)_yWS_2$ and $Rb_{0.21}(H_2O)_yWS_2$ structures[25,26]. This phenomenon was observed in all intercalated species before and after thermal treatment and thus all samples were handled using air free techniques during all characterization methods. Na intercalated 2M WS_2 powders showed similar expansion to the reported K and Rb structures with a peak at 9.53˚ for 001 peaks after 12 hours of exposure to air (SI Figure 6).

Raman spectroscopy was also used to characterize the bulk crystals through this reaction process. The intrinsic semiconducting 2H phase in the as-grown bulk crystals was confirmed by the characteristic Raman modes E^1_{2g} (in-plane) and A_{1g} (out-of-pane) at 350 cm^{-1} and 420 cm^{-1}, respectively[37] (Figure 2c). To acquire the Raman spectrum (Figure 2c) of Na intercalated 2H

WS_2, the sample was kept in an air-free homemade device to avoid any possible degradation or oxidation. The Raman spectrum of Na-intercalated 2H WS_2 is similar to that of the intrinsic 2H WS_2, with the A_{1g} Raman mode slightly shifted to a higher wavenumber. As expected, the spectrum of the thermally treated Na-intercalated 2M WS_2 exhibits much richer Raman features with several new Raman peaks, whereas the characteristic Raman modes for 2H WS_2 disappeared. While some areas of the unheated, intercalated sample showed a spectrum similar to the 2M structure, it appears to be only a surface phenomenon and full phase conversion only occurs after thermal annealing. Upong removing the sodium from the intercalated 2M WS_2, the Raman modes of the crystal are consistent with those of the previously reported results, indicating that pure 2M WS_2 was obtained[2,29]. This Raman data further confirms that the room temperature of 2H WS_2 does not convert the crystal structure to the 2M phase and only after a thermal annealing process, the 2M phase is observed by XRD and Raman.

Since the 2M phase is metastable, the intercalation was performed with MNapth at room temperature a second time[38]. The 2M was fully intercalated again following the same reaction conditions performed for the 2H WS_2 Na intercalation in the first step of the 2M WS_2 conversion process. After deintercalation, the 2M WS_2 retained its structure when observed through XRD (SI Figure 7) without any thermal treatment. This indicates that the 2M phase can be further intercalated and the intercalation process does not further change the crystal structure.

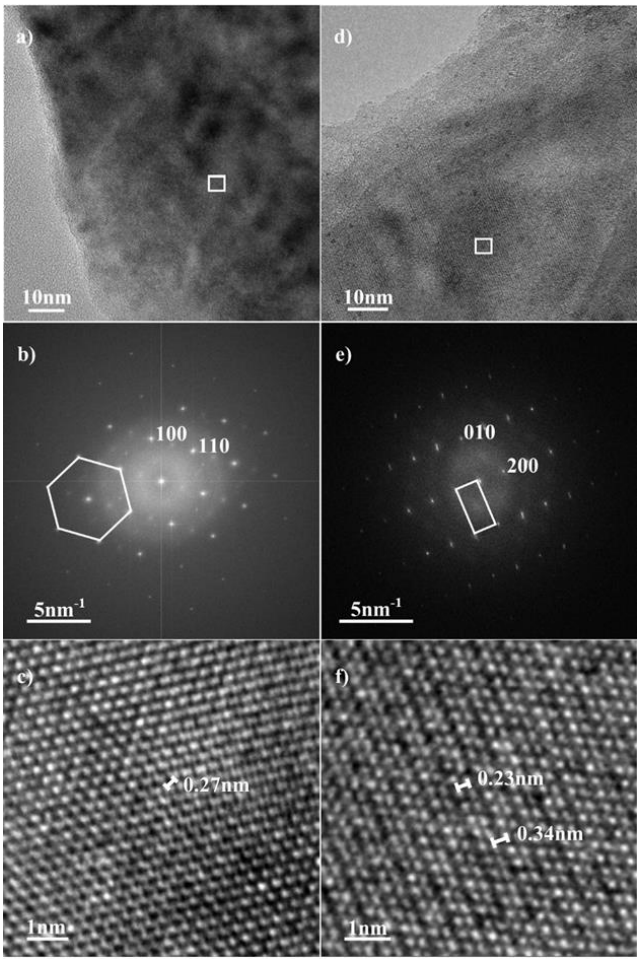

Figure 4: a) HRTEM image of 2H WS_2 thin flake b) Fourier transform of the whole 2H WS_2 thin flake c) zoomed in view of the rectangle zone in the same flake highlighting a hexagonal lattice. d) HRTEM image of 2M WS_2 thin flake e) Fourier transform of 2M thin flake and f) zoomed in view of the rectangular zone in 2M WS_2 thin flake showing characteristic zigzag chain of the 2M structure.

Figure 4(a-c) shows the hexagonal structure of the 2H crystals formed via salt flux including W atoms distances of 0.27nm and hexagonal structural pattern in Fourier transform image. These are characteristic of 2H WS_6 trigonal prisms with uniform W atom spacing consistent with previously reported literature[36].The high resolution TEM (HRTEM) image of the 2M WS_2 is also

consistent with the previously reported structure[17]. Figure 4f shows the W atom zigzag chains resulting in two different lattice fringes of 0.23 nm and 0.34 nm. This HRTEM, Fourier transform, and lattice fringe analysis further confirms that the 2H WS_2 crystals were transformed into 2M WS_2.

2M WS_2 has a known superconducting phase at approximately 8.8 K, VSM measurements allow for the elucidation of the superconducting critical temperature by means of the Meissner effect, which is identified by the change in sign of the overall magnetization of the sample, as well as a multi order of magnitude shift in magnetization between the non-superconducting regime and the superconducting regime[2,39,40].

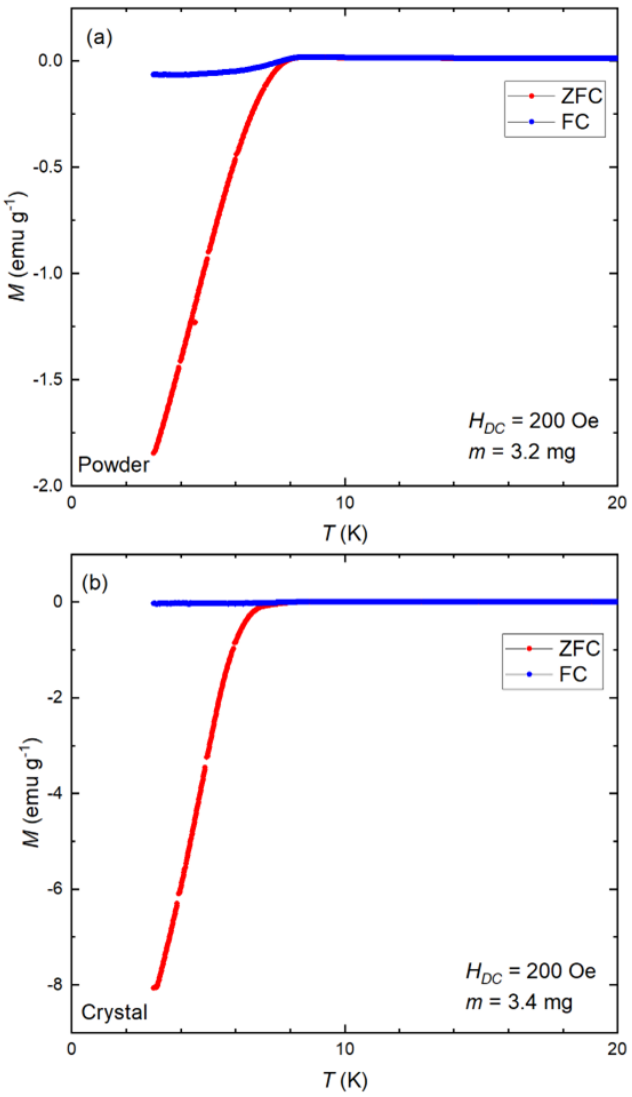

Figure 5: (a) Zero-field-cooled (ZFC) and field-cooled (FC) magnetization measurements of a powder 2M WS_2 sample with a 200 Oe applied DC magnetic field demonstrating a Tc of 8.6 K. (b) ZFC and FC measurements of a single crystal 2M WS_2 sample with a 200 Oe applied DC magnetic field showing a Tc of 8.7 K.

Magnetization measurements (Figure 5) show a distinct Meissner effect transition at 8.6 K in the powder sample and 8.7 K in the single crystal, identified from the ZFC measurements. While the Meissner effect is indicative of a transition to the superconducting regime, the broadening of

the transition is thought to be due to defects in and the crystallinity of the sample. The order of magnitude of the FC-Meissner effect transition is nearly three orders of magnitude smaller than the ZFC-Meissner effect transition, which is consistent with the two orders of magnitude change seen in the powder sample.

To further demonstrate the generality of this process, an alternate route for intercalation of 2H WS_2 was investigated using the MTEBH reducing agents. This reaction did not proceed at room temperature, however complete intercalation of alkali metals into 2H WS_2 powders (SI Figure 3,4) was confirmed after heating the MTEBH solution and WS_2 at 200°C in sealed stainless steel reaction vessels. The MTEBH is thought to follow the same process as MNapth route by transferring the alkali metals to the host WS_2 vdW region after reduction of the W.

$x[M(C_2H_5)_3BH] + WS_2 \rightarrow M_xWS_2 + B(C_2H_5)_3 + x/2\ H_2\ (g)$

M= Li, Na, K

In this route the 2H intercalated phases were easily observed through XRD analysis with the lattice constant c changing from 12.344Å to 14.463Å for Na and 15.615Å for K. EDS mapping showed a 1:3 ratio for metal intercalated 2H samples with uniform distribution of metals (SI Figure 9).

Theoretical calculation results

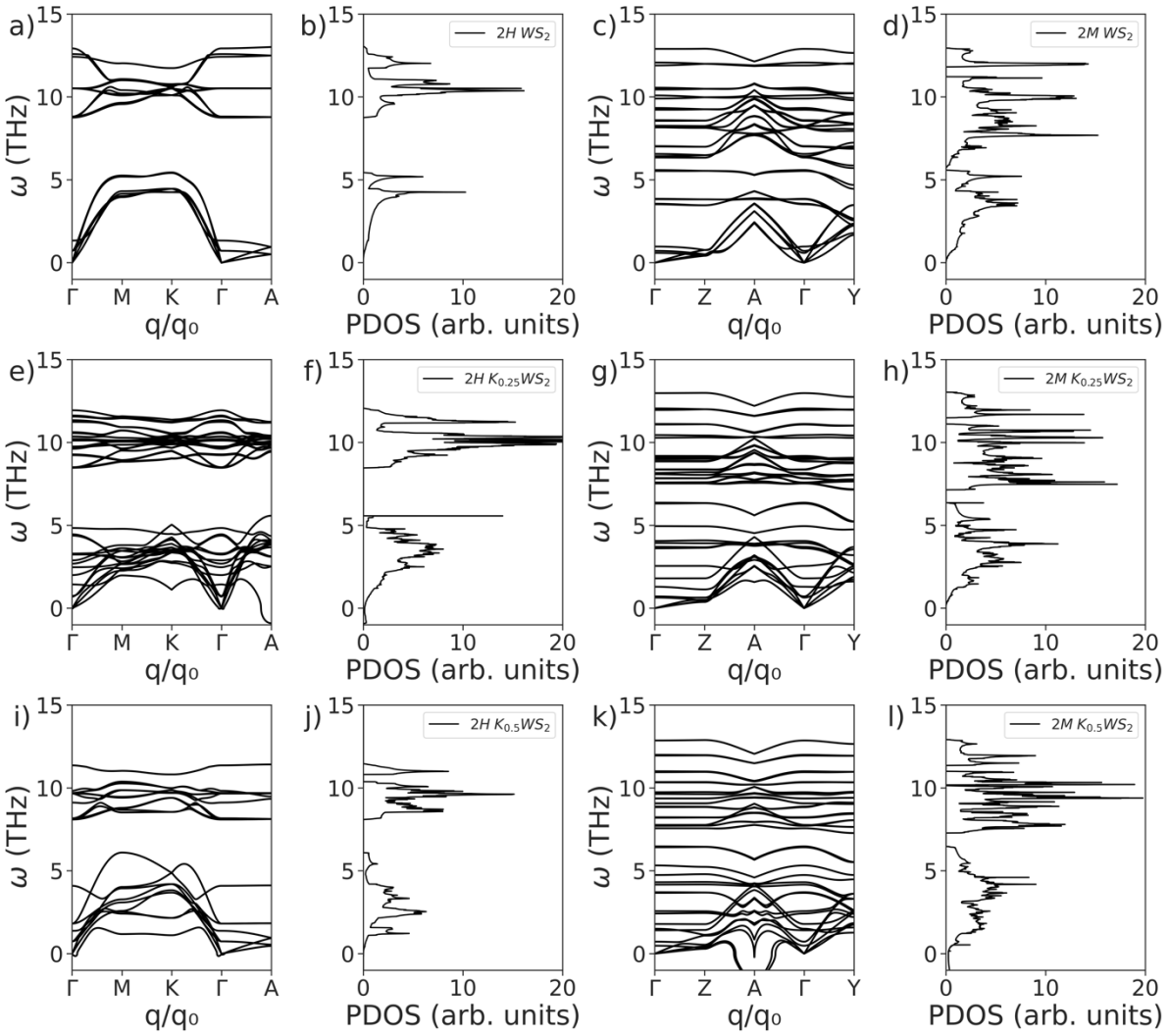

Figure 6: a) The phonon dispersion and b) density of states for 2H WS_2. c) The phonon dispersion and d) density of states for 2M WS_2. e) The phonon dispersion and f) density of states for 2H $K_{0.25}WS_2$. g) The phonon dispersion and h) density of states for 2M $K_{0.25}WS_2$. i) The phonon dispersion and j) density of states for 2H $K_{0.5}WS_2$. k) The phonon dispersion and l) density of states for 2M $K_{0.5}WS_2$.

<u>Conclusion</u>

A new synthetic process has been developed to convert 2H WS_2 powders and crystals to the highly desired 2M phase. Through this investigation, 2 unique alkali metal intercalated phases of WS_2 were observed, one with a 2H structure and after heating, one with a 2M like layered structure. These two phases were confirmed via XRD, SEM, EDS, and Raman spectroscopy providing evidence that the phase change from 2H to 2M is more complex than a simple intercalation reaction. The formation of the intercalated 2M phase is critical for the formation of the final 2M WS_2 crystals and to access this phase, a thermal annealing process is required. This process was used to generate several mm and cm sized crystals of 2M WS_2 which cannot be easily grown using traditional high temperature synthesis methods due to long heating times necessary for crystal growth. The generality of this process was demonstrated on both crystals and powders of WS_2 and further demonstrated using both alkali metal naphthalenide and alkali metal borohydride reagents. This novel synthetic process is likely general for other TMD compounds like MoS_2 or WSe_2 and could be used to gain access to other metastable phases that are not easily synthesized using traditional high temperature methods.

Displayed equations can be inserted where desired making sure they are assigned Word Style "Normal". Displayed equations can only be one column wide. If the artwork needs to be two

Supporting Information. Additional information and figures including XRD, SEM/EDS, and theoretical results are included in the supporting information which is available free of charge.

Corresponding Author

*Brian Leonard
Department of Chemistry # 3838
1000 E. University Avenue
Laramie, WY. 82071

Author Contributions

The manuscript was written through contributions of all authors. All authors have given approval to the final version of the manuscript.

Funding Sources

This research was mainly supported by the U.S. Department of Energy, Office of Basic Energy Sciences, Division of Materials Sciences and Engineering under award DE-SC0021281 and after its completion by DE-SC0024188. J.T. also acknowledges the financial support of the U.S. National Science Foundation (NSF) grant 2228841 for Raman data analysis.

Acknowledgement

This manuscript is dedicated to the memory of Frank DiSalvo who served as my advisor during a post doc fellowship at Cornell. Frank had a profound impact on everyone he worked with and his advice, mentoring, and friendship were critical when beginning my independent academic career. There are many things Frank did on a regular basis that I try to emulate with my own research group. I am forever indebted to him and cherish the time I got to spend interacting with him over the years.

This research was mainly supported by the U.S. Department of Energy, Office of Basic Energy Sciences, Division of Materials Sciences and Engineering under award DE-SC0021281 and after its completion by DE-SC0024188. J.T. also acknowledges the financial support of the U.S. National Science Foundation (NSF) grant 2228841 for Raman data analysis. The Analytical Resources Core (RRID: SCR_021758) at Colorado State University for instrument access, training, and assistance with sample analysis. The scientific computing resources of this work

were supported by the Advanced Research Computing Center (ARCC) at the University of Wyoming[43]. Wyoming Innovation Partnership (WIP) financially supported SEM and TEM analysis.

REFERENCES

(1) Britnell, L.; Ribeiro, R. M.; Eckmann, A.; Jalil, R.; Belle, B. D.; Mishchenko, A.; Kim, Y.-J.; Gorbachev, R. V.; Georgiou, T.; Morozov, S. V. Strong Light-Matter Interactions in Heterostructures of Atomically Thin Films. *Science* **2013**, *340* (6138), 1311–1314.

(2) Fang, Y.; Pan, J.; Zhang, D.; Wang, D.; Hirose, H. T.; Terashima, T.; Uji, S.; Yuan, Y.; Li, W.; Tian, Z. Discovery of Superconductivity in 2M WS2 with Possible Topological Surface States. *Adv. Mater.* **2019**, *31* (30), 1901942.

(3) Li, Y.; Wang, H.; Xie, L.; Liang, Y.; Hong, G.; Dai, H. MoS2 Nanoparticles Grown on Graphene: An Advanced Catalyst for the Hydrogen Evolution Reaction. *J. Am. Chem. Soc.* **2011**, *133* (19), 7296–7299.

(4) Radisavljevic, B.; Radenovic, A.; Brivio, J.; Giacometti, V.; Kis, A. Single-Layer MoS2 Transistors. *Nat. Nanotechnol.* **2011**, *6* (3), 147–150.

(5) Sipos, B.; Kusmartseva, A. F.; Akrap, A.; Berger, H.; Forró, L.; Tutiš, E. From Mott State to Superconductivity in 1T-TaS2. *Nat. Mater.* **2008**, *7* (12), 960–965.

(6) Song, X.; Singha, R.; Cheng, G.; Yeh, Y.-W.; Kamm, F.; Khoury, J. F.; Hoff, B. L.; Stiles, J. W.; Pielnhofer, F.; Batson, P. E. Synthesis of an Aqueous, Air-Stable, Superconducting 1T′-WS2 Monolayer Ink. *Sci. Adv.* **2023**, *9* (12), eadd6167.

(7) Torrisi, F.; Coleman, J. N. Electrifying Inks with 2D Materials. *Nat. Nanotechnol.* **2014**, *9* (10), 738–739.

(8) Ye, J. T.; Zhang, Y. J.; Akashi, R.; Bahramy, M. S.; Arita, R.; Iwasa, Y. Superconducting Dome in a Gate-Tuned Band Insulator. *Science* **2012**, *338* (6111), 1193–1196.

(9) Neto, A. C. Charge Density Wave, Superconductivity, and Anomalous Metallic Behavior in 2D Transition Metal Dichalcogenides. *Phys. Rev. Lett.* **2001**, *86* (19), 4382.

(10) Paudyal, H.; Margine, E. R. Superconducting Properties in Doped 2M-WS 2 from First Principles. *J. Mater. Chem. C* **2022**, *10* (20), 7917–7924.

(11) Zeng, H.; Dai, J.; Yao, W.; Xiao, D.; Cui, X. Valley Polarization in MoS2 Monolayers by Optical Pumping. *Nat. Nanotechnol.* **2012**, *7* (8), 490–493.

(12) Xi, X.; Wang, Z.; Zhao, W.; Park, J.-H.; Law, K. T.; Berger, H.; Forró, L.; Shan, J.; Mak, K. F. Ising Pairing in Superconducting NbSe 2 Atomic Layers. *Nat. Phys.* **2016**, *12* (2), 139–143.

(13) Fei, Z.; Palomaki, T.; Wu, S.; Zhao, W.; Cai, X.; Sun, B.; Nguyen, P.; Finney, J.; Xu, X.; Cobden, D. H. Edge Conduction in Monolayer WTe2. *Nat. Phys.* **2017**, *13* (7), 677–682.

(14) Wu, S.; Fatemi, V.; Gibson, Q. D.; Watanabe, K.; Taniguchi, T.; Cava, R. J.; Jarillo-Herrero, P. Observation of the Quantum Spin Hall Effect up to 100 Kelvin in a Monolayer Crystal. *Science* **2018**, *359* (6371), 76–79.

(15) Chen, P.; Pai, W. W.; Chan, Y.-H.; Sun, W.-L.; Xu, C.-Z.; Lin, D.-S.; Chou, M.; Fedorov, A.-V.; Chiang, T.-C. Large Quantum-Spin-Hall Gap in Single-Layer 1T′ WSe2. *Nat. Commun.* **2018**, *9* (1), 1–7.

(16) Voiry, D.; Mohite, A.; Chhowalla, M. Phase Engineering of Transition Metal Dichalcogenides. *Chem. Soc. Rev.* **2015**, *44* (9), 2702–2712.
(17) Lai, Z.; He, Q.; Tran, T. H.; Repaka, D. M.; Zhou, D.-D.; Sun, Y.; Xi, S.; Li, Y.; Chaturvedi, A.; Tan, C. Metastable 1T′-Phase Group VIB Transition Metal Dichalcogenide Crystals. *Nat. Mater.* **2021**, *20* (8), 1113–1120.
(18) Song, X.; Hoff, B.; Singha, R.; Stiles, J. W.; Skorupskii, G.; Khoury, J. F.; Cheng, G.; Kamm, F.; Uzan, A. J.; Dulovic, S. Acid-Assisted Soft Chemical Route for Preparing High-Quality Superconducting 2M-WS2. *Chem. Mater.* **2023**, *35* (14), 5487–5496.
(19) Heising, J.; Kanatzidis, M. G. Exfoliated and Restacked MoS2 and WS2: Ionic or Neutral Species? Encapsulation and Ordering of Hard Electropositive Cations. *J. Am. Chem. Soc.* **1999**, *121* (50), 11720–11732.
(20) Zhang, W.; Zhang, Y.; Qiu, J.; Zhao, Z.; Liu, N. Topological Structures of Transition Metal Dichalcogenides: A Review on Fabrication, Effects, Applications, and Potential. *InfoMat* **2021**, *3* (2), 133–154.
(21) Er, E.; Hou, H.-L.; Criado, A.; Langer, J.; Möller, M.; Erk, N.; Liz-Marzán, L. M.; Prato, M. High-Yield Preparation of Exfoliated 1T-MoS2 with SERS Activity. *Chem. Mater.* **2019**, *31* (15), 5725–5734.
(22) Zheng, J.; Zhang, H.; Dong, S.; Liu, Y.; Tai Nai, C.; Suk Shin, H.; Young Jeong, H.; Liu, B.; Ping Loh, K. High Yield Exfoliation of Two-Dimensional Chalcogenides Using Sodium Naphthalenide. *Nat. Commun.* **2014**, *5* (1), 2995.
(23) Zhu, X.; Su, Z.; Wu, C.; Cong, H.; Ai, X.; Yang, H.; Qian, J. Exfoliation of MoS2 Nanosheets Enabled by a Redox-Potential-Matched Chemical Lithiation Reaction. *Nano Lett.* **2022**, *22* (7), 2956–2963.
(24) Dines, M. B. Lithium Intercalation via N-Butyllithium of the Layered Transition Metal Dichalcogenides. *Mater. Res. Bull.* **1975**, *10* (4), 287–291.
(25) Mao, Y.; Xie, M.; Zhao, W.; Yuan, K.; Fang, Y.; Huang, F. K 0.36 (H 2 O) y WS 2: A New Layered Compound for Reversible Hydrated Potassium Ion Intercalation in Aqueous Electrolyte. *RSC Adv.* **2019**, *9* (55), 32323–32327.
(26) Mao, Y.; Fang, Y.; Wang, D.; Bu, K.; Wang, S.; Zhao, W.; Huang, F. Crystal Structure and Electrical Resistance Property of Rb0. 21 (H2O) yWS2. *Acta Crystallogr. Sect. E Crystallogr. Commun.* **2019**, *75* (7), 976–979.
(27) Benavente, E.; Santa Ana, M.; Mendizábal, F.; González, G. Intercalation Chemistry of Molybdenum Disulfide. *Coord. Chem. Rev.* **2002**, *224* (1–2), 87–109.
(28) Fang, Y.; Dong, Q.; Pan, J.; Liu, H.; Liu, P.; Sun, Y.; Li, Q.; Zhao, W.; Liu, B.; Huang, F. Observation of Superconductivity in Pressurized 2M WSe 2 Crystals. *J. Mater. Chem. C* **2019**, *7* (28), 8551–8555.
(29) Gautam, S.; McBride, J.; Scougale, W. R.; Samarawickrama, P. I.; Branco, D. D. C.; Yang, P.; Fu, Z.; Wang, W.; Tang, J.; Cheng, G. J. Controllable Superconducting to Semiconducting Phase Transition in Topological Superconductor 2M-WS2. *2D Mater.* **2023**, *11* (1), 015018.
(30) Cevallos, F. A.; Guo, S.; Heo, H.; Scuri, G.; Zhou, Y.; Sung, J.; Taniguchi, T.; Watanabe, K.; Kim, P.; Park, H. Liquid Salt Transport Growth of Single Crystals of the Layered Dichalcogenides MoS2 and WS2. *Cryst. Growth Des.* **2019**, *19* (10), 5762–5767.
(31) Kresse, G.; Furthmüller, J. Efficiency of Ab-Initio Total Energy Calculations for Metals and Semiconductors Using a Plane-Wave Basis Set. *Comput. Mater. Sci.* **1996**, *6* (1), 15–50.

(32) Kresse, G.; Hafner, J. Ab Initio Molecular Dynamics for Liquid Metals. *Phys. Rev. B* **1993**, *47* (1), 558.
(33) Kresse, G.; Furthmüller, J. Efficient Iterative Schemes for Ab Initio Total-Energy Calculations Using a Plane-Wave Basis Set. *Phys. Rev. B* **1996**, *54* (16), 11169.
(34) Grimme, S.; Antony, J.; Ehrlich, S.; Krieg, H. A Consistent and Accurate Ab Initio Parametrization of Density Functional Dispersion Correction (DFT-D) for the 94 Elements H-Pu. *J. Chem. Phys.* **2010**, *132* (15).
(35) Togo, A. First-Principles Phonon Calculations with Phonopy and Phono3py. *J. Phys. Soc. Jpn.* **2023**, *92* (1), 012001.
(36) Schutte, W.; De Boer, J.; Jellinek, F. Crystal Structures of Tungsten Disulfide and Diselenide. *J. Solid State Chem.* **1987**, *70* (2), 207–209.
(37) Zeng, H.; Liu, G.-B.; Dai, J.; Yan, Y.; Zhu, B.; He, R.; Xie, L.; Xu, S.; Chen, X.; Yao, W. Optical Signature of Symmetry Variations and Spin-Valley Coupling in Atomically Thin Tungsten Dichalcogenides. *Sci. Rep.* **2013**, *3* (1), 1608.
(38) Guan, C.; Liu, X.; Zhang, P.; Wang, S.; Fang, Y.; Chen, J.; Zhao, C.; Zhang, X.; Zhao, W.; Wang, J. High Intrinsic Phase Stability of Ultrathin 1T′ WS2. **2023**.
(39) Samarawickrama, P.; Dulal, R.; Fu, Z.; Erugu, U.; Wang, W.; Ackerman, J.; Leonard, B.; Tang, J.; Chien, T.; Tian, J. Two-Dimensional 2M-WS2 Nanolayers for Superconductivity. *ACS Omega* **2021**, *6* (4), 2966–2972.
(40) Li, Y.; Zheng, H.; Fang, Y.; Zhang, D.; Chen, Y.; Chen, C.; Liang, A.; Shi, W.; Pei, D.; Xu, L. Observation of Topological Superconductivity in a Stoichiometric Transition Metal Dichalcogenide 2M-WS2. *Nat. Commun.* **2021**, *12* (1), 2874.
(41) Botello Méndez, A. R.; Perea López, N.; Elías Arriaga, A. L.; Crespi, V.; López Urías, F.; Terrones Maldonado, H.; Terrones Maldonado, M. Identification of Individual and Few Layers of WS2 Using Raman Spectroscopy. **2013**.
(42) Chacko, L.; Massera, E.; Aneesh, P. Enhancement in the Selectivity and Sensitivity of Ni and Pd Functionalized MoS2 Toxic Gas Sensors. *J. Electrochem. Soc.* **2020**, *167* (10), 106506.
(43) Liu, F.; Rahaman, R.; Weiner, M.; Coulter, E.; Phanish, D.; Valdez, J.; Sarajlic, S.; Lara, R.; Buffington, P. Semi-Automatic Hybrid Software Deployment Workflow in a Research Computing Center. In *Practice and Experience in Advanced Research Computing*; 2023; pp 68–74.

TOC Graphic

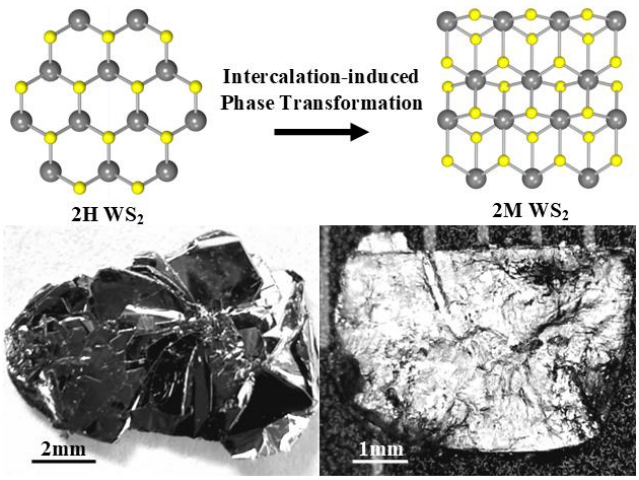
Intercalation-induced
Phase Transformation
2H WS_2
2M WS_2
2mm
1mm